Jia *et al. Cell Communication and Signaling* (2024) 22:385
https://doi.org/10.1186/s12964-024-01763-y

Cell Communication and Signaling

RESEARCH Open Access

Metabolic reprogramming and heterogeneity during the decidualization process of endometrial stromal cells

Zhaoyu Jia[1†], Yuan Wei[2†], Ye Zhang[1], Kun Song[2*] and Jia Yuan[1*]

Abstract

The human endometrial decidualization is a transformative event in the pregnant uterus that involves the differentiation of stromal cells into decidual cells. While crucial to the establishment of a successful pregnancy, the metabolic characteristics of decidual cells in vivo remain largely unexplored. Here, we integrated the single-cell RNA sequencing (scRNA-seq) datasets on the endometrium of the menstrual cycle and the maternal-fetal interface in the first trimester to comprehensively decrypt the metabolic characteristics of stromal fibroblast cells. Our results revealed that the differentiation of stromal cells into decidual cells is accompanied by increased amino acid and sphingolipid metabolism. Furthermore, metabolic heterogeneity exists in decidual cells with differentiation maturity disparities. Decidual cells with high metabolism exhibit higher cellular activity and show a strong propensity for signaling. In addition, significant metabolic reprogramming in amino acids and lipids also occurs during the transition from non-pregnancy to pregnancy in the uteri of pigs, cattle, and mice. Our analysis provides comprehensive insights into the dynamic landscape of stromal fibroblast cell metabolism, contributing to our understanding of the metabolism at the molecular dynamics underlying the decidualization process in the human endometrium.

Keywords Decidualization, Lipid metabolism, Amino acid metabolism, Human endometrium

Introduction

Decidual cells, which constitute the key components of the endometrial decidua, envelop the implanting conceptus and prepare the endometrium for embryo implantation [1–3]. These cells play a crucial role in supporting the developing embryo before placental formation, as well as providing the endometrium with mechanisms to control trophoblast invasion, maintain tissue homeostasis, and confer immunity tolerance and resistance to inflammatory signals and oxidative stress [4, 5]. Under the influence of increasing progesterone levels and local cAMP production, elongated fibroblast-like endometrial stromal cells undergo differentiation into rounded and specialized secretory epithelioid decidual cells—a process referred to as decidualization [6–8]. The pivotal

†Zhaoyu Jia and Yuan Wei contributed equally to this work.

*Correspondence:
Kun Song
songkun2001226@sdu.edu.cn
Jia Yuan
Jia.Yuan@sdu.edu.cn
[1]Advanced Medical Research Institute, Cheeloo College of Medicine, Shandong University, Jinan 250012, Shandong, China
[2]Department of Obstetrics and Gynecology, Qilu Hospital of Shandong University, Jinan 250012, Shandong, China

role of decidual cells in establishing and maintaining pregnancy cannot be overstated, as any disruption to the decidualization process may lead to a range of pregnancy complications, including implantation failure, pregnancy loss, infertility, impaired endometrial receptivity, recurrent miscarriages, placental abruption, and intrauterine fetal growth restriction [9, 10].

Decidualization of the human endometrium is characterized by substantial morphological and functional changes in human endometrial stromal cells, leading to the differentiation of stromal cells into metabolically active decidual cells [8, 11]. This process has a high energy demand, requiring significant reprogramming of energy metabolism, including carbohydrate, lipid, and amino acid metabolism, to support decidual cell differentiation [12]. As a result, there is a heightened demand for glucose, which enters the glycolytic system to generate energy molecules. Decidual cells demonstrate increased glucose uptake and low-glucose conditions have been shown to suppress production of decidual prolactin (PRL) [13]. Blocking the pentose phosphate pathway inhibits decidualization of endometrial stromal cells both in vitro and in vivo [14].

Aside from carbohydrates, lipids play a critical role in providing energy for metabolism and maintaining homeostasis. Lipids are evenly distributed in the peri-implantation uterus to supply raw materials and energy for the stromal-decidual transformation [12]. Disruption of sphingolipid metabolism leads to instability in the uterine vascular bed, and impaired decidualization [15, 16].

During the process of implantation, the decidua undergoes differentiation into various regions: the decidual basalis, located beneath the implantation site, the adjacent decidua parietalis, and the more distant decidual secretory endometrium. The latter remains similar to the pre-decidualized endometrium, indicating potential heterogeneity in the characteristics of decidual cells [5, 17, 18]. The use of transcriptome profiling at the single-cell level provides invaluable information on cell-to-cell variability, potential subpopulations, rare cell types, functional possibilities, and activities of major metabolic pathways [19, 20]. Recently, analysis at the single-cell level has revealed different subpopulations of human decidual cells in early pregnancy [21]. Additionally, Bao et al. identified a glycolytic subtype of decidual cells in the decidua of patients with recurrent miscarriage [22].

In this study, we aimed to investigate the metabolic characteristics of endometrial stromal cells and decidual cells by analyzing integrated single-cell RNA sequencing (scRNA-seq) datasets. We sought to identify and characterize the metabolic heterogeneity between sub-clusters of stromal cells and decidual cells, respectively. The findings from this study may offer new insights into the development and maintenance of the decidua, as well as the intricate communication between decidual cells and trophoblast cells.

Materials and methods

Data collection and processing

The scRNA-seq datasets of human endometrium across the natural menstrual cycle were downloaded from Gene Expression Omnibus database under accession number GSE111976; scRNA-seq datasets of the human first trimester fetal-maternal interface were downloaded from ArrayExpress database under the accession number E-MTAB-6701. GSE111976 and E-MTAB-6701 were integrated and removed batch effect by harmony R package. The standard workflow of cell clustering in Seurat was utilized [23]. Cells with fewer than 500 detected genes and for which the total mitochondrial gene expression exceeded 15% were removed. Genes expressed in fewer than three cells were removed. Doublets were removed using DoubletFinder. Cell cycle analysis was done with CellCycleScoring function in Seurat R package. To identify differentially expressed genes among samples and different clusters, the FindMarkers function with the Wilcoxon rank-sum test algorithm was used under the following criteria: logfc. threshold > 0.25, min.pct > 0.25.

Bulk expression profiles of pig, mouse and cattle endometrium were downloaded from Gene Expression Omnibus database under accession number GSE48862, GSE43667, GSE46732 and GSE19140, respectively. Differential expression genes of GSE46732 and GSE19140 were obtained by using limma R package [24]. For GSE48862, analysis of differential gene expression was performed with edgeR R package. And analysis of differential gene expression of GSE43667 was performed with DESeq R package [25]. P value < 0.05 and adjusted p value < 0.05 were considered to be statistically significant.

Constructing cell pseudotime trajectories

Pseudotime trajectory analysis was performed separately for the decidual and stromal cells using Monocle2 [26]. Genes expressed in fewer than ten cells were removed. We used differentialGeneTest function to identify significant genes. And we used reduceDimension function and orderCells function to construct cell trajectory. For decidual cell sub-clusters, we used Slingshot R package v2.6.0 to identify the global lineage structure with a cluster-based minimum spanning tree (MST) and fit simultaneous principal curves to describe each lineage.

Functional enrichment analysis

Gene Ontology (GO) analysis and Kyoto Encyclopedia of Genes and Genomes (KEGG) analysis were performed using clusterProfiler R package [27]. The terms which p value < 0.05 were selected. Gene Set Enrichment Analysis

(GSEA) was also implemented with clusterProfiler R package. The gene set of "c2.all.v7.5.1.entrez" from the Molecular Signature Database was utilized as the reference set. And the p value cutoff was equal 0.05.

Cell-cell communication analysis

Two R packages, iTALK, NicheNet, were used to inferring the cell-cell communication between trophoblast cells and decidual cells [28, 29]. Based on scRNA-seq data, iTALK can characterize, compare and illustrate intercellular communication signals. NicheNet can predict ligand-target networks between interacting cells and infer their activity.

CellChat

For detailed exploration of cell-cell communication between trophoblast cells and decidual cells, we used CellChat R package for further analysis [30]. We followed the standard workflow, using identifyOverExpressedGenes function to get the over expressed genes and computeCommunProb function to get the potential intercellular communication.

MEBOCOST

The inference of metabolite meditated cell-cell communication between trophoblast cells and decidual cells was performed using MEBOCOST python package [31]. We transformed the Seurat object to Scanpy object and followed the standard MEBOCOST workflow (https://github.com/zhengrongbin/MEBOCOST).

Trophoblast trajectory inference

To ascertain the pseudotime trajectory of trophoblast cell sub-clusters, we used Slingshot R package v2.6.0 [32]. Using Slingshot function, we identified the global lineage structure with a cluster-based minimum spanning tree (MST) and fitted simultaneous principal curves to describe each lineage.

Next, we used the partition-based graph abstraction (PAGA) method wrapped in Scanpy python package v1.9.1 to construct the pseudotime trajectory of trophoblast cell sub-clusters by generating graph-like maps of cells to support our Slingshot results [33].

Analysis of gene sets activities

To quantify the activities of specific gene sets in individual cells, we employed the irGSEA R package. This package incorporates rank-based gene set enrichment analysis for single cells and provides easily interpretable results. Specifically, the irGSEA.score function was utilized to obtain the specific gene set scores for each cell, using the default parameters. To visualize the outcomes, we utilized the irGSEA.density.scatterplot function. The gene sets used in the analysis were obtained from the Molecular Signatures Database (MSigDB).

Transcription regulation analysis of metabolic cell clusters

In order to analyze the underlying transcription factors and their target genes which regulated stromal cells and decidual cells of different metabolic clusters, we used pySCENIC python package to access the activity of these genes in individual cells [34]. Co-expression modules were inferred by using grnboost2 function. Then the indirect targets from these modules were pruned by using cis regulatory motif discovery. Aucell function was used to quantify the activity of these transcription factors and their target genes by enrichment scores.

Human sample collection

Secretory endometrium and decidua samples were obtained from Department of obstetrics and gynecology, Qilu Hospital, Shandong University. Secretory endometrium samples were obtained from hysterectomy specimens of patients who were in reproductive age (18–40) with normal menstrual cycles. These patients underwent hysterectomy due to stage I cervical cancer or benign gynecological diseases such as uterine fibroids and adenomyosis. Decidua were obtained from terminations of pregnancies between 24 and 37 weeks-gestation. Ethics approval for the collection and use of human endometrial samples was authorized by the Ethics Committee Review Board of Qilu Hospital, Shandong University (Permit No. KYLL-202203-011). All the recruited participants gave their written informed consent.

RNA extraction and RT-qPCR

Total RNA was extracted from the tissues with Trizol reagent (Invitrogen Life Technologies, USA). 1ug of RNA was reverse transcribed into cDNA using Evo M-MLV RT Kit with gDNA Clean for qPCR II (Accurate Biology, China). RT-qPCR was performed using ChamQ SYBR qPCR Master Mix (Vazyme, China) on Light Cycler 96 Instrument (Roche, Switzerland). ACTB was selected as internal control. Primer sequences are provided in Supplementary Table 1.

Western blot

Tissues were lysed in RIPA buffer (Beyotime, P0013B) supplemented with 1% protease inhibitor (Roche, 04693132001) and centrifugated for 10 min at 12,000 rpm. The protein concentration was determined using a Pierce BCA Protein Assay Kit (Thermo, 23,227) to ensure equal loading of protein across different samples. 20 μg of protein was loaded for each sample, proteins were separated by 10% sodium dodecyl sulfate-polyacrylamide gel electrophoresis (SDS-PAGE) and transferred to a polyvinylidene difluoride (PVDF) membrane (Millipore,

ISEQ00011). After transfer, the membrane was blocked with 5% fat-free milk for 1 h at room temperature and subsequently incubated with the indicated primary antibodies, followed by the corresponding horseradish peroxidase (HRP)-conjugated secondary antibodies. Blots were visualized using an ECL kit (Thermo, 32,106) and detected by the Amersham Imager 680 System (Chemiluminescence). The following antibodies were used in this study: DHRS3 (15393-1-AP, diluted 1:1000, Proteintech), PSAP (10801-1-AP, diluted 1:1000, Proteintech), PLPP1 (160,691, diluted 1:1000, ZEN-BIOSCIENCE), GPX1 (381,587, diluted 1:1000, ZEN-BIOSCIENCE), MAOB (12602-1-AP, diluted 1:1000, Proteintech), MGST1 (R22577, diluted 1:1000, ZEN-BIOSCIENCE), GLUL (11037-2-AP, diluted 1:1000, Proteintech), β-ACTIN (20536-1-AP, diluted 1:3000, Proteintech) and Goat Anti-Rabbit IgG H&L(HRP) (ab205718, diluted 1:5000, Abcam). Quantification was performed using ImageJ.

Multiplex immunohistochemistry (mIHC)

Multiplex immunohistochemistry was performed using an Opal Multiplex fIHC kit (Akoya Biosciences, Marlborough, MA). In brief, after baking for 2 h at 60℃, FFPE slides were deparaffinized and rehydrated in gradient alcohol successively. The tissue slides were then subjected to heat-induced epitope retrieval using Tris-EDTA buffer (C1034, Solarbio, pH = 8.0) for 20 min, then washed with 1xTBST buffer (T1082, Solarbio) and blocked non-specific binding with 30% goat serum for 1 h. Next, the slides were incubated overnight with primary antibodies of two panels, including CK8 (Cat: MABT329, diluted 1:500, Sigma-Aldrich), DHRS3 (Cat: 15393-1-AP, diluted 1:100, Proteintech), PSAP (Cat: 10801-1-AP, diluted 1:100, Proteintech), and PLPP1 (Cat: 160,691, diluted 1:100, ZEN-BIOSCIENCE); CK8 (Cat: MABT329, diluted 1:500, Sigma-Aldrich), GPX1 (Cat: 381,587, diluted 1:100, ZEN-BIOSCIENCE), MAOB (Cat: 12602-1-AP, diluted 1:100, Proteintech), MGST1 (Cat: R22577, diluted 1:100, ZEN-BIOSCIENCE) and GLUL (Cat: 11037-2-AP, diluted 1:100, Proteintech), respectively. Rabbit IgG (B900610, diluted 1:200, Proteintech) was selected as negative control. The slides were incubated for 20 min with corresponding HRP-conjugated second antibodies (Opal Anti-Ms + Rb HRP, Cat: ARH1001EA; HRP-conjugated Affinipure Goat Anti-Rat IgG(H + L), Cat: SA00001-15), sequentially stained with tyramide signal amplification and Opal fluorophore (NEL811001KT, Akoya Biosciences). Opal detector fluorophores were applied to each marker in the following order: Opal-480, Opal-690, Opal-620, Opal-540; Opal-480, Opal-650, Opal-540, Opal-620, Opal-690. After all antigens were labeled with different antibodies, DAPI (C1002, Beyotime) was used for nuclei staining. The slides were sealed in Anti-Fade Fluorescence Mounting Medium (Cat: ab104135, Abcam). Multispectral panoramic tissue scanning microscopy (TissueFAXS Spectra, TissueGnostics) was then used for scanning the stained slides.

Construction of phylogenetic tree and analysis of gene conservation

Phylogenetic trees were constructed using coding sequences (CDS) by concatenation. The CDS of genes involved in metabolic pathway in FASTA format were download form NCBI database. SeqKit was used to sort the FASTA sequences, and MAFFT was used for multiple sequence alignment [35, 36]. The results of multiple sequence alignment were trimmed by trimAI. After concatenating by PhyloSuite, we used IQ-TREE to constructed the phylogenetic trees and visualized the trees using ggtree [37, 38].

NCBI taxonomy common tree was constructed by Common Tree tool of NCBI Taxonomy database and visualized using iTOL online tool [39].

Gene involved in the specific metabolism pathway were download from the KEGG database. And the species conservation data for genes were obtained from HomoloGene database with gene symbol as queries. The species evolution tree was constructed by using Common Tree tools in the Taxonomy database.

Metabolic pathway maps were constructed according to pathway maps of KEGG database.

Statistical analysis

Statistical analyses were conducted using GraphPad Prism (v6.0) for RT-qPCR results, and R (v4.2.2) along with RStudio (2023.12.0) for bioinformatics data. Data are presented as mean ± SEM. Comparisons between groups were performed using Student's t-tests and Wilcoxon rank-sum tests. $P < 0.05$ was considered statistically significant. The RT-qPCR and WB results were analyzed using Student's t-test. For the bioinformatics data, differentially expressed genes between cells in different samples and clusters were identified using the Wilcoxon rank-sum test.

Results

Unveiling metabolic programming during decidualization via comprehensive integration of scRNA-seq data

We utilized single-cell sequencing (scRNA-seq) data to examine the metabolic characteristics of endometrial stromal fibroblast cells, revealing significant alterations in metabolic programming during decidualization (Fig. 1A). We downloaded two 10x single-cell RNA sequencing datasets from the GEO and ArrayExpress databases under the accession numbers GSE111976 [40] and E-MTAB-6701 [21], respectively. We integrated the two datasets and removed batch effects using the harmony R package [41]. After quality control and filtration, we

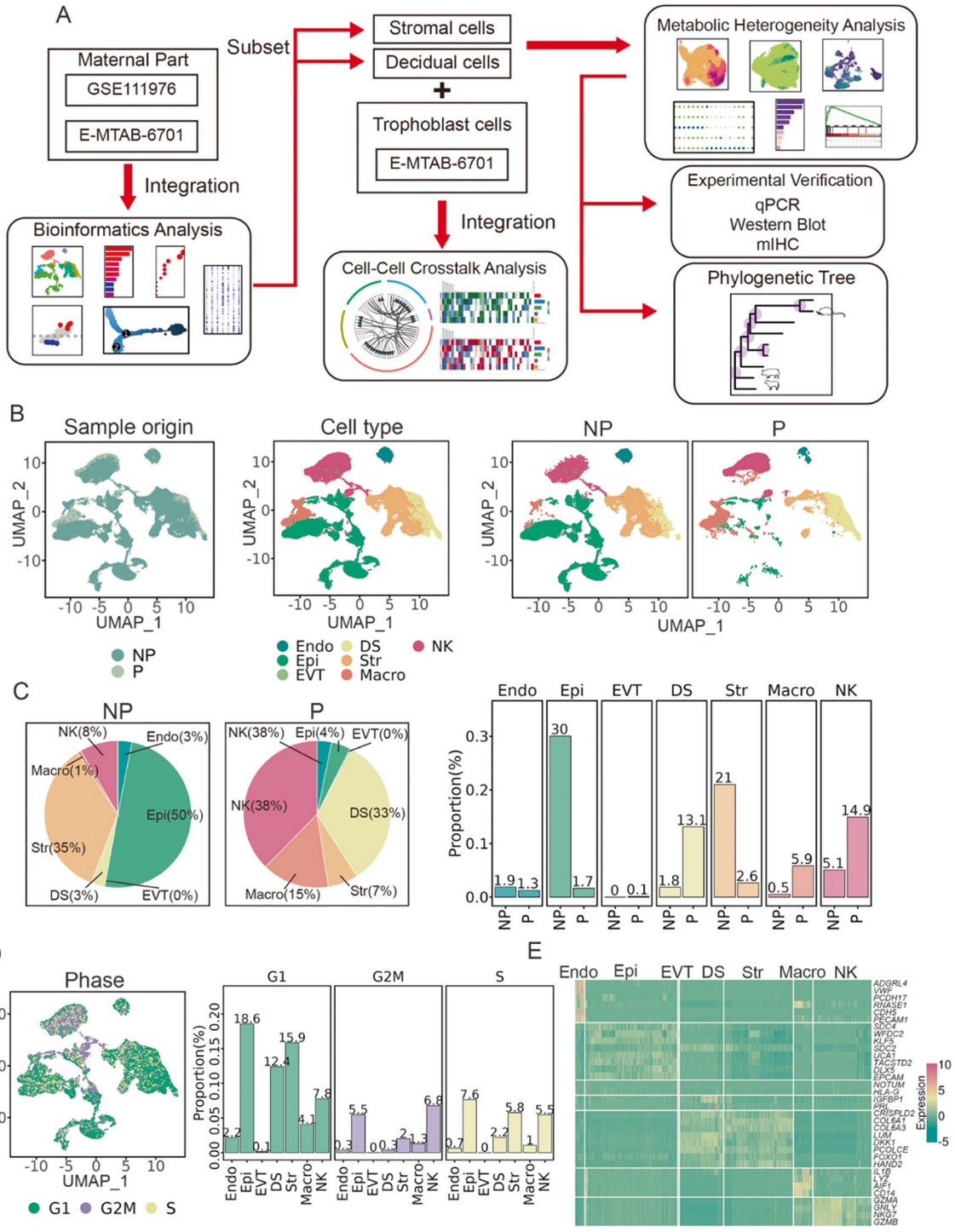

Fig. 1 Overview of single-cell annotation in the endometrium during the menstrual cycle and early pregnancy in humans. **A** Schematic representation of the entire research workflow. **B** UMAP visualization of endometrium cells with its sample type of origin (Pregnancy or Non-pregnancy) and the associated cell types, 7 cell clusters of endometrium were identified and annotated based on canonical marker genes. Endo, endothelial cell; Epi, endometrial epithelial cell; DS, endometrial decidual stromal cell; Str, endometrial stromal cell; Macro, macrophage; NK, nature killer cell; EVT, extravillus trophoblast; N: non-pregnancy; P: pregnancy. **C** The proportion of each cell type in non-pregnant and pregnant endometrium. **D** The cell cycle analysis of each cell type in endometrium. **E** Expression of classical marker genes of each cell type in the endometrial samples

included 91,327 cells from 24 individuals in this research. Following graph-based clustering, we annotated 7 main cell clusters using known marker genes (Fig. 1B). Stromal fibroblast cells were abundant in both pregnant decidua and non-pregnant endometrium (Fig. 1C). Cell cycle analysis revealed that most stromal fibroblast cells were in the G1 phase, with a few in the S or G2M phase (Fig. 1D). Stromal fibroblast cells were divided into two cell clusters (decidual cells and stromal cells) based on specific cell markers. They all expressed *LUM* and *HAND2*, and only decidual cells expressed marker genes of decidualization (*IGFBP1*, *PRL*) (Fig. 1E, Fig. S1A).

According to the clustering results, we identified 2,303 significantly differentially expressed genes (DEGs) by comparing the gene expression levels of decidual cells with stromal cells (Fig. 2A). We obtained 1,590 human metabolic genes from 93 metabolic pathways in the Kyoto Encyclopedia of Genes and Genomes (KEGG) database. By overlapping DEGs with metabolic genes, we identified 157 metabolic DEGs (Fig. 2B). Further exploration of metabolic pathways using KEGG analysis revealed significant changes, particularly in oxidative phosphorylation (Fig. 2C). Gene Ontology (GO) analysis indicated that the metabolism-associated DEGs were functionally enriched in terms related to purine nucleotide metabolic processes and ribose phosphate metabolic processes (Fig. 2D).

Additionally, we observed significant changes in terms associated with lipid and amino acid metabolism: The sphingolipid metabolism, biosynthesis of amino acids, glutathione metabolism, and arginine metabolism were up-regulated significantly in decidual cells compared to stromal cells (Fig. 2E). Consistent with previous studies, genes related to glycolysis/gluconeogenesis were significantly induced during decidualization [42]. Our Gene Set Enrichment Analysis (GSEA) results also demonstrated that decidual cells significantly up-regulated genes associated with amino acid, lipid, and carbohydrate metabolism-associated pathways (Fig. 2F, Fig. S1B).

To provide a more comprehensive and intuitive view of the changes in metabolic pathway activity during decidualization, we utilized the singscore method within the irGSEA R package to score the activity of specific gene sets in individual cells and visualize it on UMAP embeddings. Our observations revealed that decidual cells exhibited elevated activity in lysine degradation, histidine metabolism, glutathione metabolism, alanine, aspartate, and glutamate metabolism, sphingolipid metabolism, tryptophan metabolism, arginine and proline metabolism, cysteine and methionine metabolism compared to stromal cells (Fig. 2G). These results indicate that when stromal cells undergo decidualization, their metabolic profiles undergo dramatic alterations, especially in amino acid metabolism, suggesting overall changes.

Metabolic heterogeneity exists in decidual cells with differentiation maturity disparities

In most mammals that exhibit decidualization, the endometrial stromal cells undergo decidualization only after embryo implantation. However, in humans, stromal cells differentiate into secretory epithelioid-like decidual cells during the mid-secretory phase of the menstrual cycle [1, 2, 7].

In our exploration of the metabolic characteristics and distinctions among decidual cell populations, we initially compared the metabolism of decidual cells in pregnant and non-pregnant women. This analysis unveiled 17 subpopulations of decidual cells: D_c0 to D_c16 (Fig. 3A), with pseudotime analysis indicating a maturation gradient, showing that pregnant decidual cells tend to be more mature towards the end of the pseudotime axis (Fig. S2A). Genes related to hormone response, blood vessel development, and receptor tyrosine kinase signaling increased with pseudotime, while those associated with the HIF-1 signaling pathway and IGF transportation decreased (Fig. S2B). Differential expression analysis identified 2,395 genes that distinguished pregnant from non-pregnant decidual cells (Fig. 3B), including 172 involved in metabolism (Fig. 3C). These metabolic genes were implicated in processes such as purine-containing compound metabolism, monosaccharide metabolism, sphingolipid metabolism, and cellular amino acid metabolism via GO analysis (Fig. 3D). KEGG analysis underscored enrichment in pathways like sphingolipid metabolism, cysteine and methionine metabolism, glutamate metabolism, and glutathione metabolism (Fig. 3E). Moreover, GSEA results accentuated enrichment in pyruvate, amino acid, and lipid metabolism signatures in pregnant decidual cells compared to non-pregnant ones (Fig. S2C). Overall, these findings suggest that the metabolic pathway of decidual cells from pregnant females appears to be more active than that of non-pregnant females.

D_c6 exhibited the highest degree of differentiation among the sub-populations and expressed key decidualization markers like *IGFBP1* and *PRL* (Fig. S3). Slingshot was employed to construct a pseudotime trajectory to explore the differentiation pathway of decidual clusters. This involved assigning D_c4 as the initial cell state, and D_c6 as the terminal state. The analysis revealed three main developmental trajectories (Fig. 3F). Decidual markers increased along pseudotime in trajectories 1 and 2, indicating a deepening decidualization process (Fig. 3G). Furthermore, decidual cells with hierarchical differentiation and maturity display different metabolic pathway activities. D_c3, which has a high degree of decidualization, showed higher activity in sphingolipid metabolism. Nevertheless, D_c5 and D_c2, at the initial stage of decidualization, exhibited high activity in pathways such as cysteine and methionine metabolism,

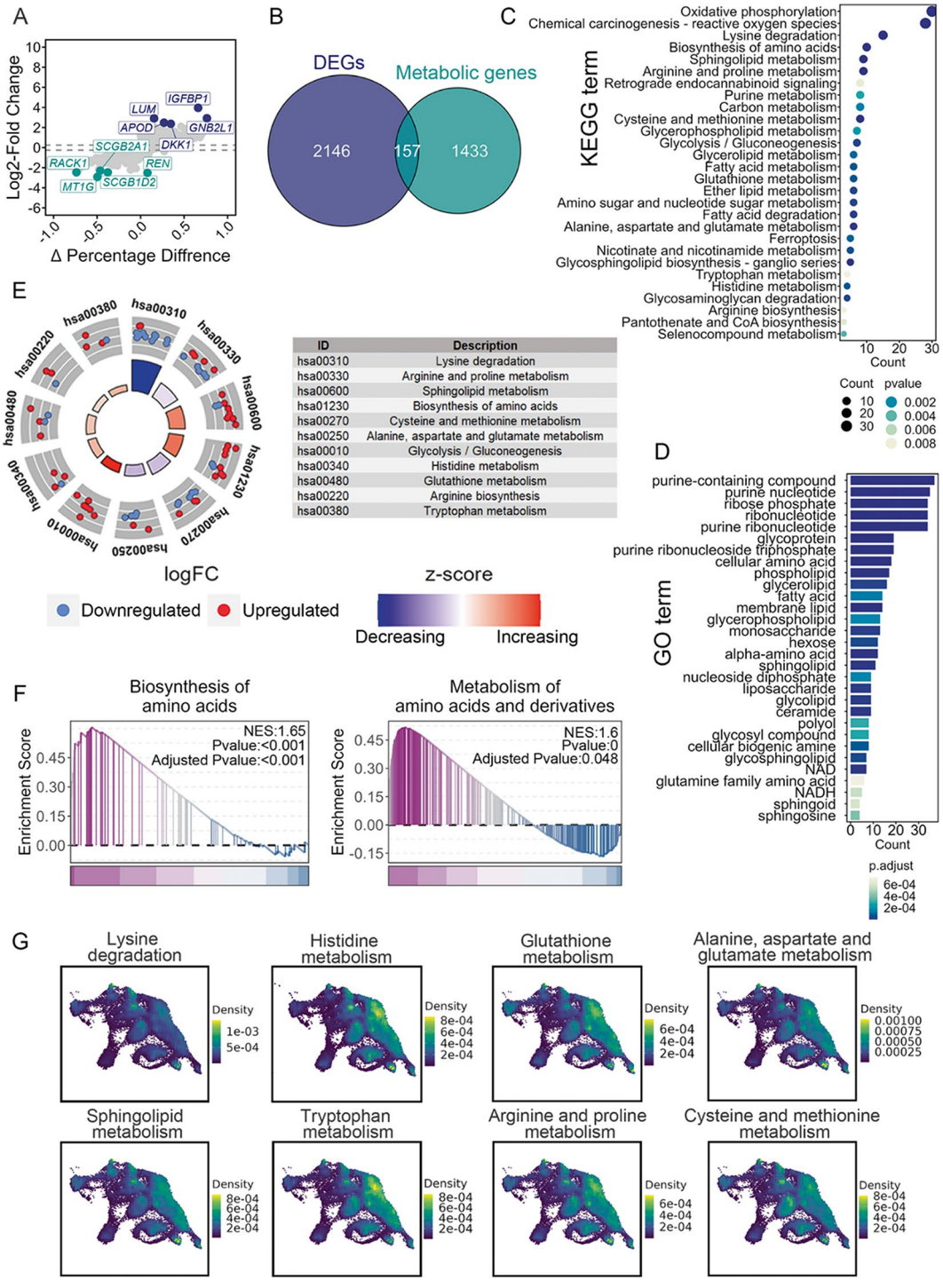

Fig. 2 The metabolic reprogramming of decidualization. **A** Volcano plots depicting the expression levels of differentially expressed genes between stromal cells and decidual cells. **B** Venn diagram showing the overlapping genes between differentially expressed genes (DEGs) and metabolic genes from the Kyoto Encyclopedia of Genes and Genomes (KEGG) pathway database. **C** and **D** Functional enrichment of metabolic DEGs: and KEGG enrichment (C) GO enrichment (D). **E** Circle plot displaying selected metabolism-related KEGG terms. **F** Gene Set Enrichment Analysis (GSEA) plot showing high expression of amino acid metabolism-related genes in decidual cells compared to stromal cells. **G** Distribution of selected metabolic pathway activity scores in stromal and decidual cells on UMAP.

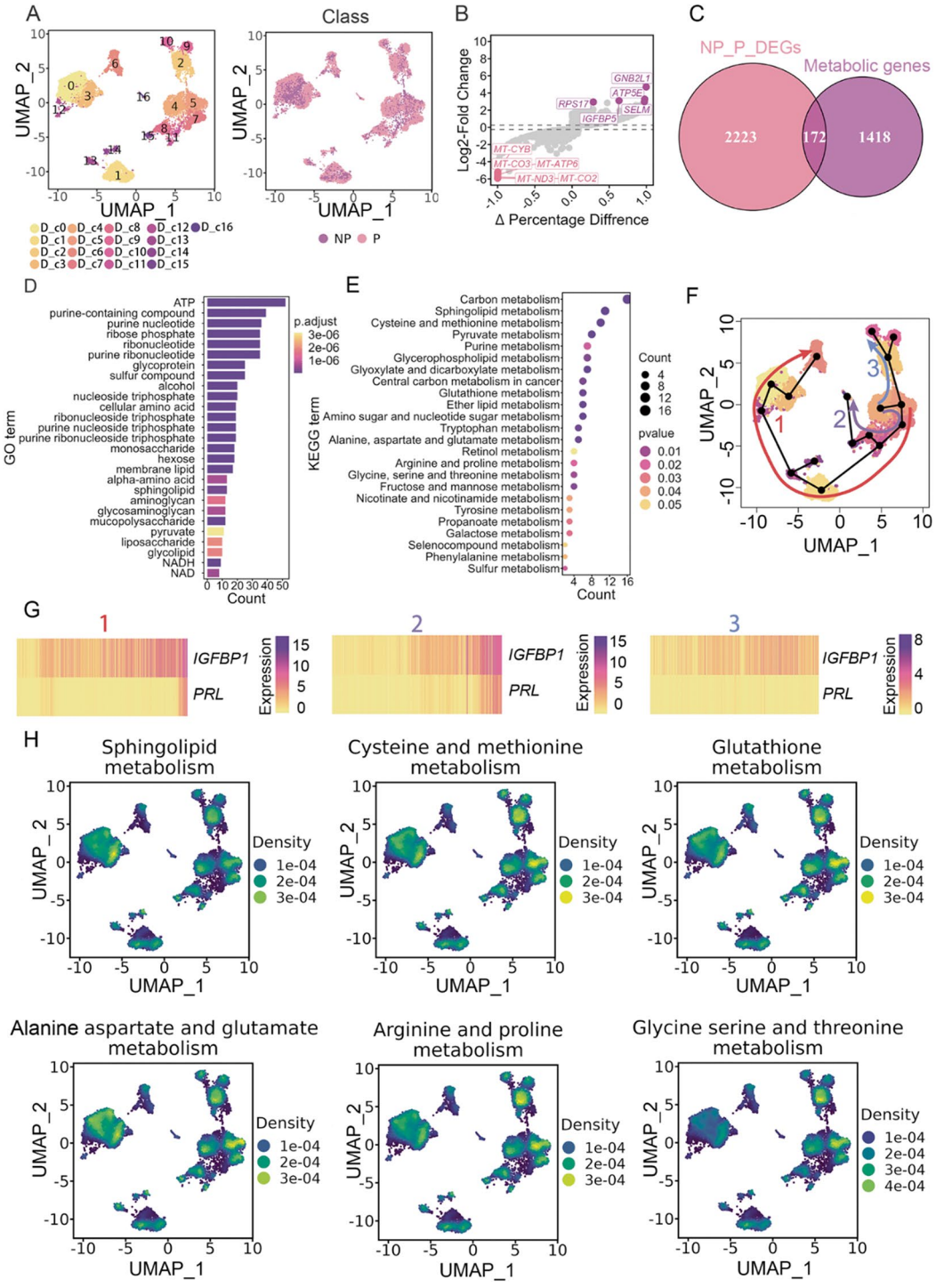

Fig. 3 Metabolic heterogeneity among decidual cell sub-clusters. **A** UMAP plots of decidual cells colored by cell sub-clusters and by sample groups. **B** Volcano plot of DEGs between non-pregnant decidual cells and pregnant decidual cells. **C** Venn diagram showing the overlapping genes between DEGs and metabolic genes from the KEGG database. **D** GO enrichment of metabolic DEGs between non-pregnant decidual cells and pregnant decidual cells. **E** KEGG enrichment of metabolic DEGs between non-pregnant decidual cells and pregnant decidual cells. **F** Pseudotime analysis reveals three branches with different evolutionary trajectories. **G** The expression of *IGFBP1* and PRL in three Pseudotime trajectories. **H** Distribution of selected metabolic pathway activity scores in decidual cell sub-clusters.

glutathione metabolism, and arginine and proline metabolism. Additionally, the alanine, aspartate, and glutamate metabolism pathway exhibited comparable activity across all decidual cells (Fig. 3H). These findings underscore significant metabolic differences in decidual phases, highlighting metabolic heterogeneity among decidual cell sub-clusters. In addition, we observed significant changes in the metabolic characteristics of stromal cells during the proliferative phase, secretory phase, and pregnancy (Fig. S4). When stromal cells transition from the proliferative phase to the secretory phase, genes associated with lipid metabolism and amino acid metabolism are activated. Furthermore, we found that an increase in the activity of VEGFA-VEGFR2 signaling pathway in stromal cells along the pseudotime order (Fig. S5). These results indicate a rise in the metabolic level of stromal cells from the proliferative phase to secretory phase (Fig. S6).

Based on the above results, we next investigated the expression pattern of these metabolic pathways in human endometrial samples. First, we analyzed the expression of genes known to be critical for amino acid metabolism and lipid metabolism by Quantitative real-time PCR (RT-qPCR). The expression levels of *MAOB*, *GLUL*, *GPX1*, *PLPP1*, *DHRS3*, *PSAP*, and *MGST1* were found to be higher in decidual samples than in endometrial samples during the secretory phase (Fig. 4A), as confirmed by Western blotting results (Fig. 4B). This suggests that these genes play a role in the decidualization process. Moreover, Multiplex immunohistochemistry demonstrated that these key genes are highly expressed in different sub-clusters of decidual cells (Fig. 4C). It is also important to note that some of our qPCR results do not match the single-cell sequencing analysis results. According to the single-cell sequencing data analysis, some metabolic-related genes have high expression levels in other cell types of the endometrium (Fig. S7). Specifically, CKB, CNDP2, RIMKLB, and ASRGL1 exhibit high expression levels in epithelial cells, while SAT1 and PGAM1 also show high expression levels in endothelial cells. The human samples we used are a mixture of multiple cell types. Consequently, the gene expression levels may be influenced by the abundant epithelial and endothelial cells in the human endometrium, leading to discrepancies with the sequencing results; Moreover, significant individual differences among humans can lead to inconsistencies, as reflected in the WB results. Nevertheless, the dramatic alterations in the metabolic profiles of stromal cells during decidualization are evident. These findings contribute to our understanding of the metabolism at the molecular dynamics of underlying the decidualization process in the human endometrium.

Decidua cells with different metabolic characteristics manifest varied cellular functional activities

We next hypothesized that decidual cells with distinct metabolic characteristics perform specific physiological functions. We utilized metabolism-related genes from the KEGG database to reconstruct the expression matrix of decidual and re-clustered these cells by reducing dimensionality. We employed the top 20 ranked markers in KEGG enrichment analysis, the highest-ranking term determined the name of the metabolic sub-clusters (Fig. 5A). KEGG analysis revealed that C2 and C3 were closely associated with oxidative phosphorylation. Consequently, we clustered decidual cells into four metabolic clusters characterized by arginine and proline metabolism, oxidative phosphorylation, purine metabolism, and thermogenesis (Fig. 5B). Mapping the metabolic sub-clusters back to the sub-clusters of decidual cells revealed a distinct division based on metabolic genes. Cells within each metabolic sub-cluster exhibited a relatively concentrated distribution (Fig. 5C). Specifically, sub-clusters D_c0 and D_c3 of decidual cells were clustered into the arginine and proline metabolism cluster; sub-clusters D_c6 into the thermogenesis cluster; sub-clusters D_c1 into the oxidative phosphorylation cluster; and sub-clusters D_c2, D_c4, D_c5, D_c8, D_c9, and D_c10 into the purine metabolism cluster. Moreover, the pseudotime trajectory depicted a developmental path of decidual cell metabolic subtypes, revealing a differentiation relationship from cells in the purine metabolism cluster to the arginine and proline metabolism cluster, and ultimately to the oxidative phosphorylation cluster and thermogenesis cluster (Fig. 5D and E).

Transcription factors (TFs) serve as the most direct regulators of cell fate and can be employed to reprogram cells into new cell fates. The analysis of transcription factor activity indicated that each decidual metabolic sub-cluster exhibited specific and highly active transcription factors. Notably, the cells in the thermogenesis cluster showed high activity in transcription factors. *KLF16*, *ZNF518A*, *TAF1*, and *RFX1* were active in the oxidative phosphorylation cluster, *EOMES* and *ZBTB17* were active in the arginine and proline metabolism cluster, while *SPI1*, *GATA4*, and *SIRT6* were active in the thermogenesis cluster (Fig. 5F). We conducted gene set scoring to assess the partial functions of cells in each metabolic cluster. The cluster characterized by arginine and proline metabolism exhibited the highest activity, with high scores for each gene set. The purine metabolism cluster exhibited the second highest level of activity. In contrast, the other two clusters demonstrated notably elevated activity in angiogenesis, cytokine secretion, and the regulation of epithelial cell proliferation (Fig. 5G). Our analysis also delineated six distinct stromal cell sub-clusters with well-defined metabolic signatures, providing

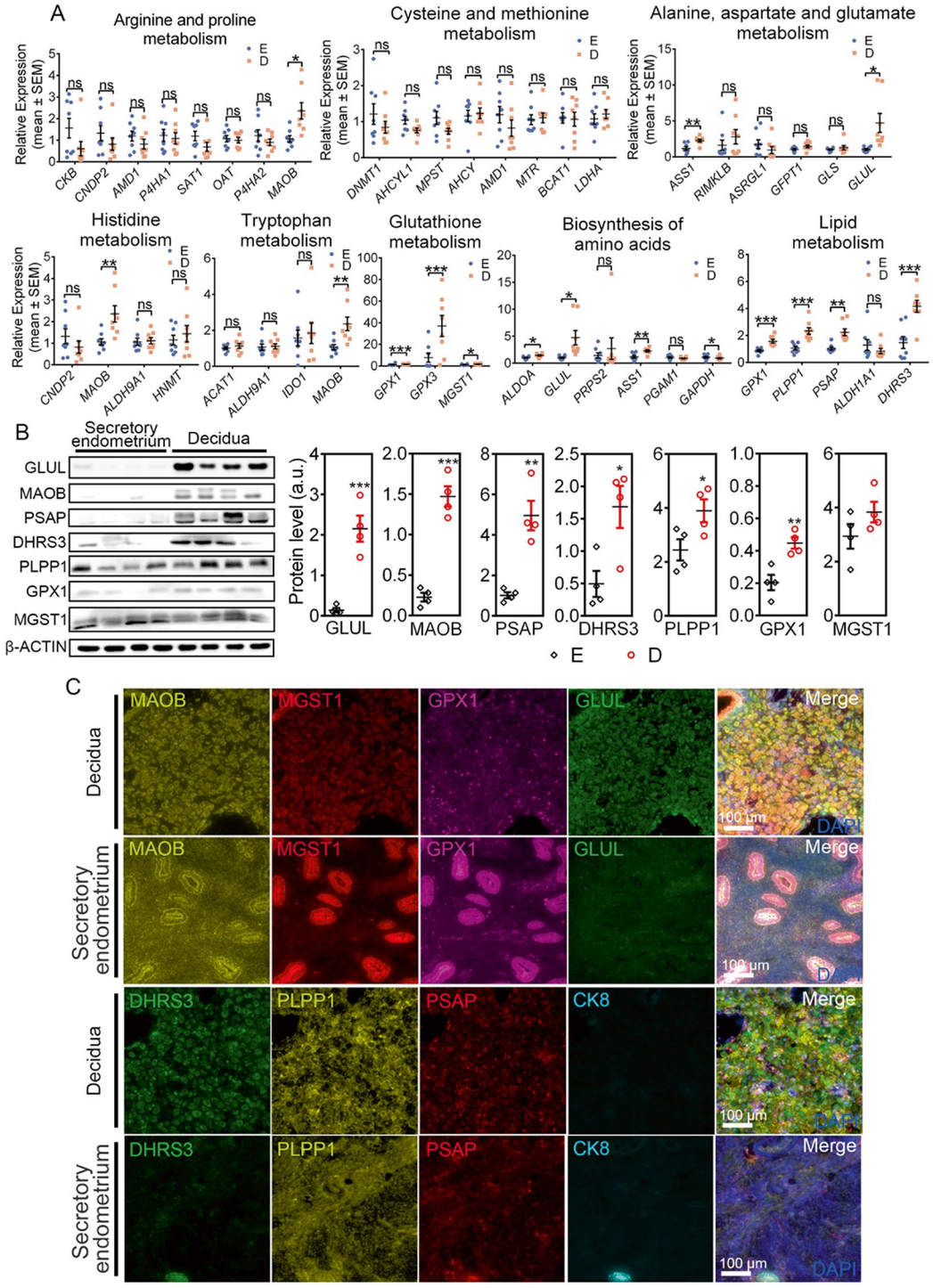

Fig. 4 Differential Expression of Amino Acid Metabolism and Lipid Metabolism-Associated Genes Between Decidua and Stroma. **A** mRNA expression levels of genes involved in amino acid metabolism and lipid metabolism pathways between secretory endometrium and decidua of early pregnancy examined by RT-qPCR (n = 8 per group). E, secretory endometrium; D, decidua. Data are presented as the mean ± SEM. *P < 0.05, **P < 0.01, ***P < 0.001. **B** Western blot analysis and quantitation of the protein level of key genes involved in amino acid and lipid metabolism (n = 4 per group). **C** Representative multiplex immunohistochemical images of the protein level of amino acid metabolic genes (GPX1, MGST1, MAOB, GLUL) and lipid metabolic genes (PLPP1, PSAP, DHRS3) in normal decidua (n = 2).

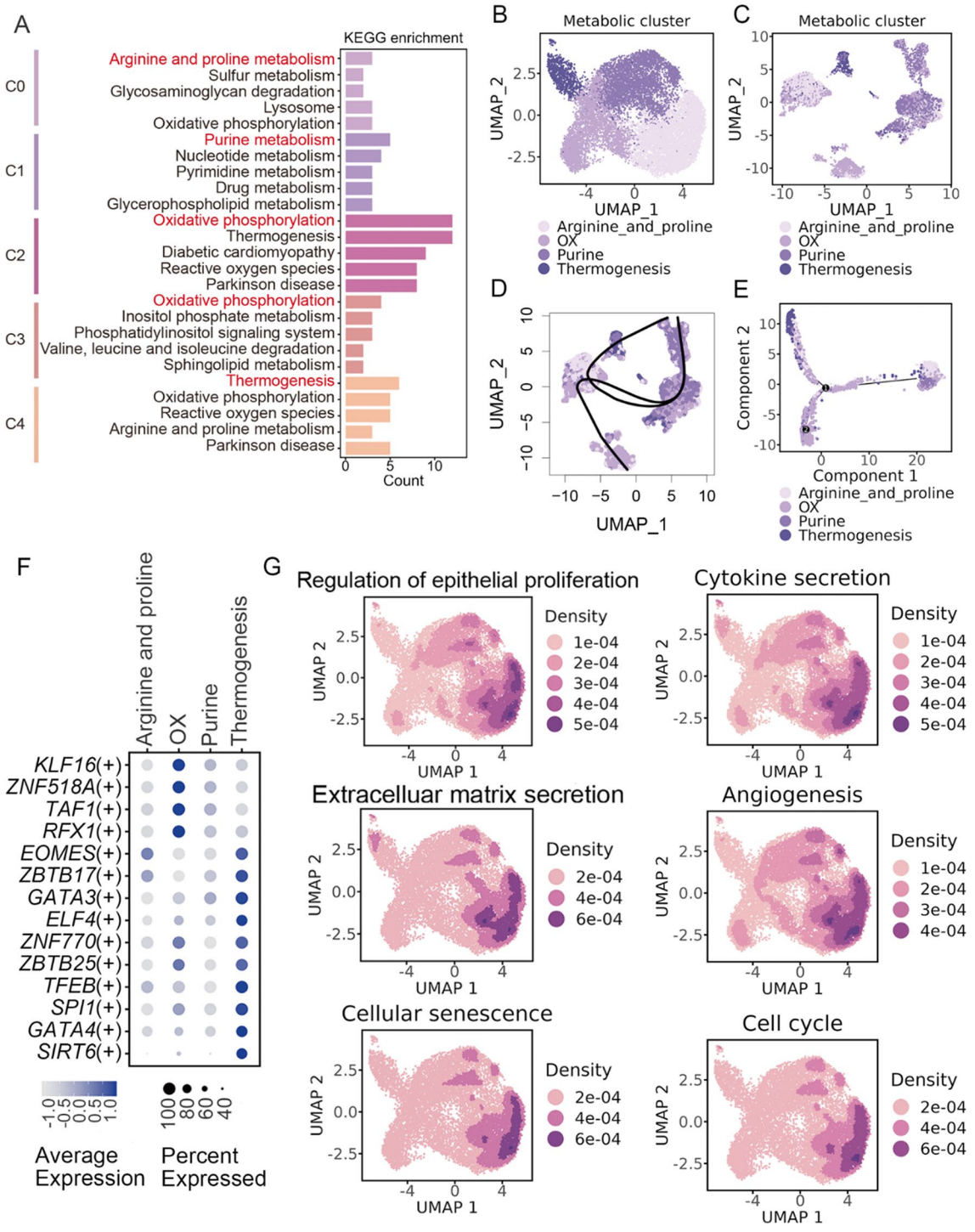

Fig. 5 Decidua cells in different metabolic sub-clusters exhibit different cellular and transcription factor activities. **A** Kyoto Encyclopedia of Genes and Genomes (KEGG) analysis for top 20 (if available) significant enriched metabolic marker genes in 5 metabolic clusters of decidual cells. **B** UMAP plots showing the metabolic clusters of decidual cells. The color of each dot indicates the dominant metabolic process of each cell. **C** The metabolic landscape of decidual cells in the context of 17 original decidual cell populations. The dot was colored based on the dominant metabolic process. **D** and **E** Pseudotime trajectory showing the developmental trajectories of 4 decidual metabolic clusters. **F** The area under the curve (AUC) scores of transcription factors of each metabolic cluster estimated by SCENIC. **G** Distribution of cell hallmark process activity scores in different decidual metabolic clusters.

comprehensive insights into the dynamic landscape of stromal cell metabolism (Fig. S8).

Cell-cell communications show diversity and selectivity in decidual and trophoblast cells with unique metabolic traits

Decidua shields the fetus from the maternal immune system, regulates trophoblast invasion, maintains placenta development and maturation [1, 2, 11]. To analyze the crosstalk between decidual cells and trophoblast cells, we found that different trophoblast cells have varying interactions with various decidual cells (Fig. S9). Referred to Arutyunyan, Anna et' study [13], we conducted a more detailed grouping of trophoblast cells from E-MTAB-6701 [21] (Fig. S10A). Trophoblast subclusters were annotated by canonical markers (Fig. S10B). The pseudotime trajectories performed by Slingshot and PAGA proved that our cell annotation is basically correct (Fig. S10C, D). And the detailed annotation was used in following analysis (Fig. S10E and F).

Initially, we investigated the intercellular communication among various cell types comprehensively. The D_c15 and D_c16 sub-clusters of decidual cells received the highest number of signals. D_c0, D_c3, D_c5, D_c11, D_c13, D_c14, D_c15, and D_c16 sent a high number of signals. Among these clusters, those with a large number of cells (D_c0, D_c3, D_c5) exhibited higher metabolic pathway activity. Most trophoblast cells sent fewer signals, but the invasive extravillous trophoblast cell (iEVT) and giant cells (GC) sent more signals than other trophoblast cell clusters (Fig. 6A). Along the differentiation pathway from the villous cytotrophoblast (VCT), cytotrophoblast cell column VCT (VCT-CCC) to iEVT and GC, the strength of signals sent and received by cells continued to increase. The syncytiotrophoblast (SCT) appeared to be the least active cluster in communication with other cells. Among the sender cell populations, D_c0, D_c3, and D_c5 were the most active. D_c2 also showed a tendency to send signals but weaker than the others (Fig. 6B). For a detailed breakdown of sending and receiving signals, for example, PRL signals were primarily sent by D_c6 and received by D_c0 and D_c3, and all decidual cells sent PSAP signals, which were received by iEVT and GC. ANGPTL signals were also sent by all decidual cells and mainly received by VCT-CCC, iEVT, and GC. D_c8, D_c10, and D_c13 sent VISFATIN signals to VCT-CCC, iEVT, and GC. The expression levels of receptors involved in VISFATIN signals increased along the pseudotime order of trophoblast cells. (Fig. 6C and D).

The ligand of VISFATIN signal, NAMPT, was mainly secreted by Dc_8, D_c10, and D_c13, and it was sent to the iEVT and GC cluster (Fig. S11A and B). PSAP was secreted by all the decidual clusters and trophoblasts, and its receptor GPR37 was expressed on iEVT and GC (Fig. S11C and D). ANGPTL2, which is a member of ANGPTL protein family, was predominantly secreted by D_c2 and D_c5. And ITGA5, the receptors of ANGPTL2 was mainly expressed in iEVT and GC (Fig. S11E and F). These results indicate that decidual cells with different metabolic features send different signals and may communicate with different trophoblast cell clusters.

In the same vein, we combined decidual cells with trophoblast cells to investigate potential variations in cell-to-cell communication among them, particularly in different metabolic clusters. In summary, cells with distinct arginine and proline metabolic profiles were observed to be the primary signal senders and receivers (Fig. 6E). Notably, the cluster linked to arginine and proline metabolism emerged as the most dynamic group of sender cells, showing a stronger tendency to transmit signals rather than receive them. (Fig. 6F). For incoming signaling patterns, cells involved in oxidative phosphorylation and thermogenesis appeared to receive fewer signals, with relatively weaker signal strength. The arginine and proline metabolism cluster received the most signals, including MK, PTN, CD99, SPP1, GAS, PRL, PROS, GDF, and PTPRM. Cells in the purine metabolism cluster primarily received COLLAGEN, MK, PTN, SPP1, and GALECTIN signals (Fig. 6G). Regarding outgoing signaling patterns, the arginine and proline metabolism cluster sent signals such as COLLAGEN, MK, CD99, VISFATIN, THBS, GAS, TENASCIN, FGF, and PROS, while the purine metabolism cluster sent CD99, VISFATIN, THBS, and FGF signals (Fig. 6H).

NAMPT was predominantly secreted by the purine cluster and arginine and proline metabolism cluster and sent to the iEVT and GC cluster (Fig. S11G and H). PSAP was mainly secreted by all the decidual clusters and trophoblasts, with its receptor GPR37 being expressed on iEVT and GC (Fig. S11I and J). ANGPTL2 was primarily secreted from the purine cluster and arginine and proline metabolism cluster. iEVT and GC were the primary receiving cell for ANGPTL2 signal by expressing ITGA5 (Fig. S11K and L).

We employed MEBOCOST to infer metabolite-mediated cell-cell communication events. By estimating the relative abundance of metabolites based on the gene expression of metabolic reaction enzymes, we determined the number of metabolite-sensor communications for all cell clusters. For trophoblast cells, VCT-fusing, VCT-p and VCT-CCC cells seem to have the most number of senders and receivers; iEVT cells expressed the fewest receivers. For decidual cells, D_c0 and D_c3 sent more metabolites, and D_c3 received more signals. D_c6 sent and received fewer signals (Fig. 7A). Decidual cells had more connections and higher scores with VCT-p and VCT-CCC (Fig. 7B). *ADRA2C* was highly expressing in D_c0 and *ABCG2* was highly expressing in iEVT and

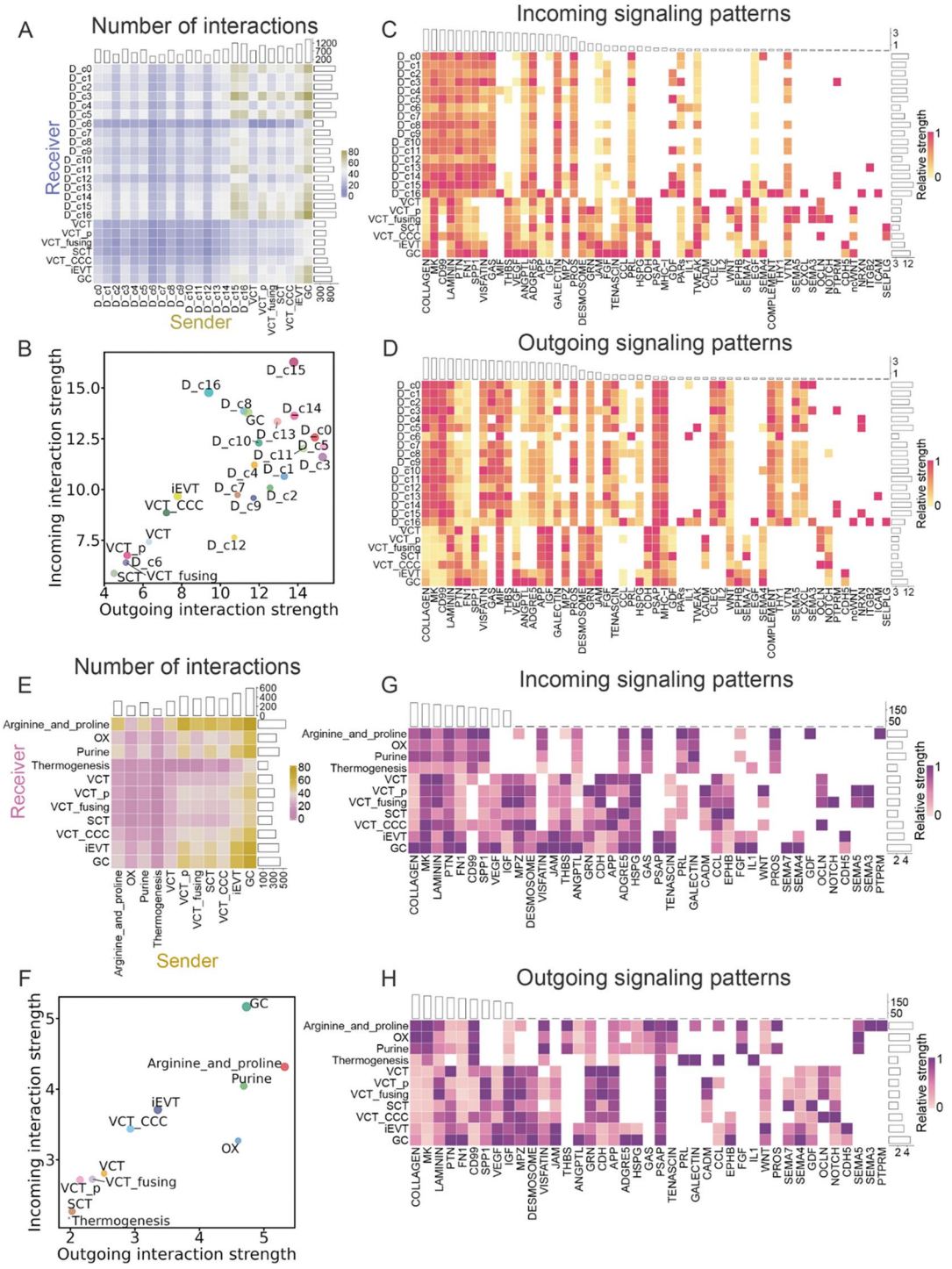

Fig. 6 The cell-cell communication between decidual cells with different metabolic characteristics and trophoblast cells exhibits heterogeneity. **A** The number of interactions between decidual and trophoblast cell sub-clusters. **B** Visualization of the dominant senders (sources) and receivers (targets) using a scatter plot. **C** Heat map showing signals contributing the most to incoming signaling of all the cell sub-clusters. **D** Heat map showing signals contributing the most to outgoing signaling of all the cell sub-clusters. **E** The number of interactions between decidual metabolic clusters and trophoblast cell sub-clusters. **F** Visualization of the dominant senders (sources) and receivers (targets) using a scatter plot. **G** Heat map showing signals contributing the most to incoming signaling of decidual metabolic clusters and trophoblast cell sub-clusters. **H** Heat map showing signals contributing the most to outgoing signaling of decidual metabolic clusters and trophoblast cell sub-clusters.

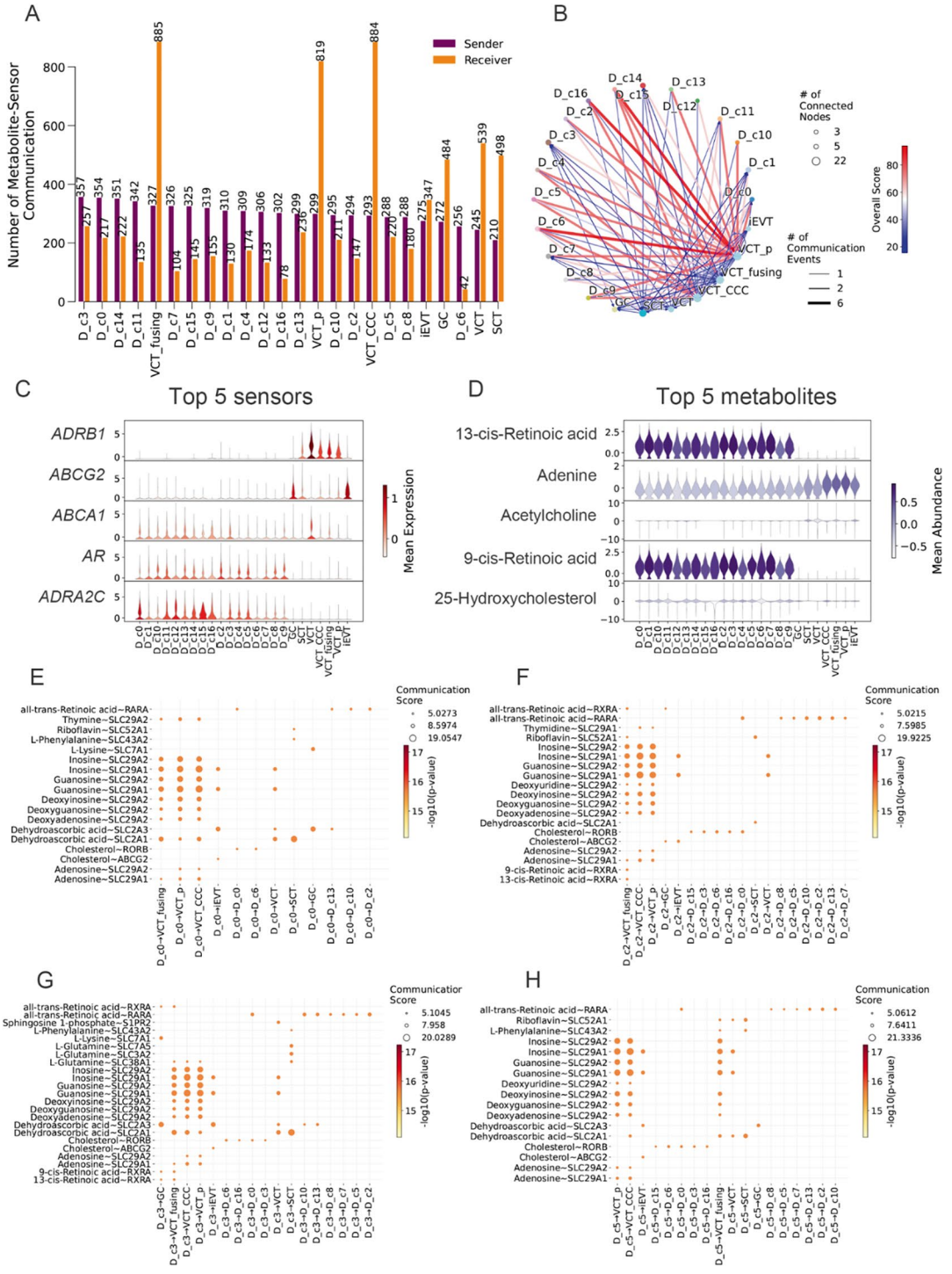

Fig. 7 D_c0, 3 with high metabolic activity send more metabolites, and D_c3 receives more signals. **A** Number of communications of each cell type (including 17 decidual cell clusters and 7 types of trophoblast cells). **B** Summary of communication in cell-to-cell communication network. **C** Violin plot shows the expression of top 5 sensors in communication. **D** Violin plot shows the top 5 estimated abundance of metabolites in communication. **E-H** Dot map shows detailed communications between decidual cell clusters and trophoblast cell clusters. The sender focus on D_C0 (E), D_C2 (F), D_C3 (G), D_C5 (H). By expressing SLC29A1 and SLC29A2, VCT-p, VCT-fusing and VCT-CCC received inosine, guanosine and three deoxynucleosides sent by D_c0, 2, 3, 5. D_c3 with high expression level of genes involved in sphingolipids metabolism and alanine, aspartate and glutamate metabolism sent glutamine to SCT and sent sphingosine 1-phosphate to VCT.

GC (Fig. 7C). Cis-retinoic acid was abundant in decidual cells and all the cell clusters had high level of adenine (Fig. 7D). In line with our previous findings, D_c3, characterized by a high expression level of genes associated with sphingolipid metabolism and alanine, aspartate, and glutamate metabolism, sent glutamine to SCT and sphingosine 1-phosphate to VCT (Fig. 7E-H). Next, we analyzed the metabolic communication between decidual cells in different metabolic clusters and trophoblast cells. Among decidual cells, the OX cluster sent more metabolites, while the arginine and proline metabolism cluster received more signals. The thermogenesis cluster both sent and received fewer signals. Given our earlier results, we focused on metabolites secreted by the arginine and proline metabolism cluster and the purine metabolism cluster. VCT-p, VCT-fusing, and VCT-CCC received inosine, guanosine, and four deoxynucleosides from the arginine and proline metabolism cluster and purine metabolism cluster, as indicated by the expression of SLC29A1 and SLC29A2 (Fig. S12).

Conservation of metabolic characteristics among mammals during pregnancy

The preceding results demonstrate significant alterations in lipid metabolism and amino acid metabolism within stromal cells during the process of decidualization in women. Notably, both decidual cells and stromal cells exhibit their distinctive metabolic profiles. This prompts us to investigate whether similar changes occur in other mammalian species and if the functional aspects of these metabolic pathways remain consistent. To address this inquiry, we collected and analyzed four publicly available datasets (GSE48862 [43, 44], GSE43667 [45], GSE46732 [46], GSE19140 [47]). We identified differentially expressed metabolic genes (Fig. S13A) and performed KEGG enrichment analysis (Fig. S13B). Our analysis revealed significant alterations in sphingolipid in pig endometrial tissues and amino acid metabolism in both pig and cattle endometrial tissues during the transition from non-pregnant phase to pregnant phase. Furthermore, we observed notable disparities in sphingolipid and amino acid metabolism between cyclic and pregnant endometrial stroma in pigs, as well as between the stromal cells surrounding the decidua and those within the inter-implantation decidua in mice.

We constructed phylogenetic trees for three different datasets involving genes related to alanine, aspartate, glutamate metabolism, glutathione metabolism, and sphingolipid metabolism. The selected 10 species of organisms for this analysis were: *Bos taurus* (Bos), *Cavia porcellus* (Cavia), *Felis catus* (Felis), *Homo sapiens* (Homo), *Macaca mulatta* (Macaca), *Mus musculus* (Mus), *Ornithorhynchus anatinus* (Ornithorhynchus), *Oryctolagus cuniculus* (Oryctolagus), *Rattus norvegicus* (Rattus), and *Sus scrofa* (Sus). We used the maximal likelihood (ML) method to construct the phylogenetic tree and validated its accuracy using the Shimodaira–Hasegawa-like approximate likelihood ratio test (SH-aLRT). Before the ML analysis, we employed ModelFinder to determine the best-fit model of nucleotide substitution for each dataset. The selected models were as follows: SYM+I+G4 for the concatenated dataset related to alanine, aspartate, and glutamate metabolism; TIM3+F+I+G4 for the concatenated dataset associated with glutathione metabolism; and TVM+F+I+G4 for the concatenated dataset for sphingolipid metabolism. The high degree of gene sequence conservation, as evidenced by the relationships depicted in the phylogenetic tree, strongly suggests functional conservation in these metabolic pathways across placental mammals (Fig. S14A).

The analysis of gene conservation underscores the prevalence of gene preservation within metabolic pathways in mammals (Fig. S14B). Notably, in the alanine, aspartate, and glutamate metabolism pathway, all genes remain conserved within the Catarrhini group; Within the sphingolipid metabolism pathway, gene conservation is observed within the Boreoeutheria group. Furthermore, the sphingosine biosynthesis pathway and ceramide biosynthesis pathway exhibit conservation within the broader Eukaryota category; The sphingosine degradation, hydrolysis of galabiosylceramide, and hydrolysis of sphingomyelin pathways are preserved within the Bilateria group; Genes associated with the lactosylceramide biosynthesis, sulfoglycolipids biosynthesis, hydrolysis of lactosylceramide, and hydrolysis of galactosylceramide sulfate pathways demonstrate conservation within the Euteleostomi group; Genes involved in the glutamine metabolism pathway are conserved within the Euarchontoglires group; The 5-oxoproline metabolism pathway enjoys preservation within the broader Eukaryota category; Finally, the glutathione biosynthesis pathway remains conserved within the Bilateria group (Fig. S15).

In conclusion, our analysis reveals that the metabolic pathways associated with glutamate, glutamine, and sphingolipids undergo significant alterations across numerous mammalian pregnancies (Fig. 8). Importantly, these metabolic pathways exhibit a high degree of conservation, suggesting their pivotal role in the context of all mammalian pregnancies.

Discussion

Stromal cells are known to present variations in the decidualization process, encompassing differences in differentiation rates and spatial characteristics. The phenotypic specialization is influenced by metabolic heterogeneity triggered by both hormonal and embryonic signals. However, the identification of subpopulations

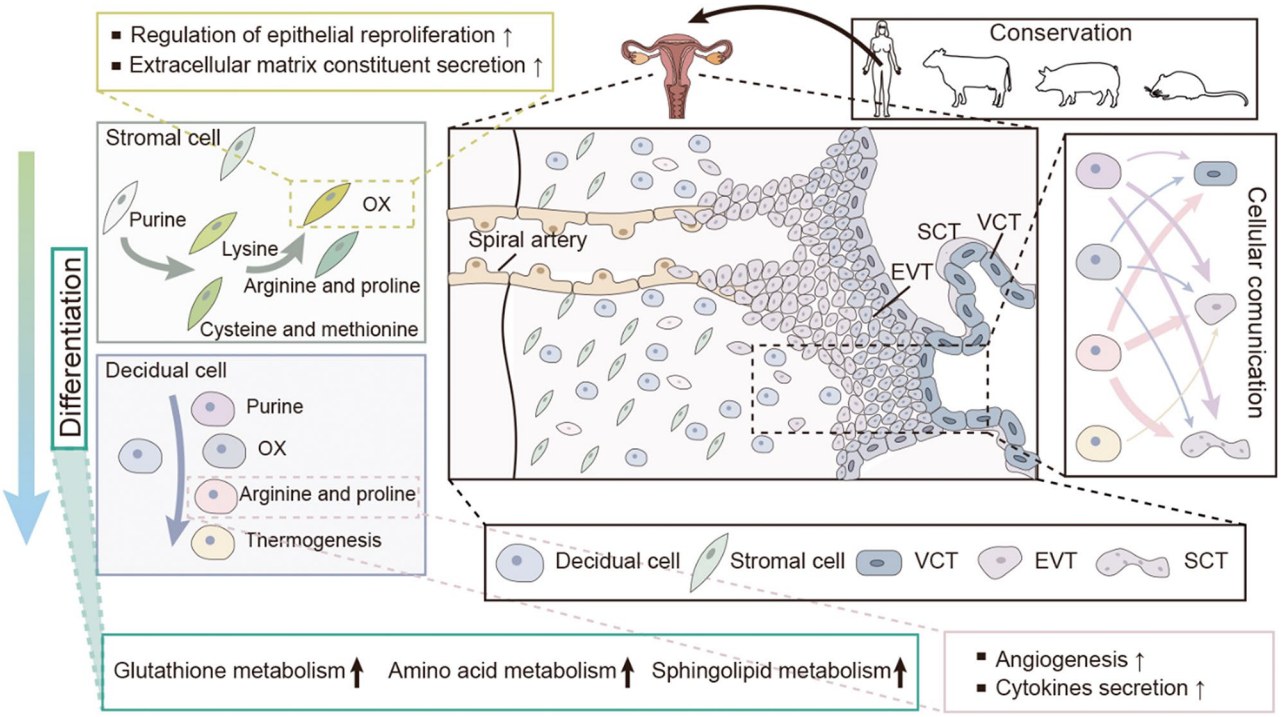

Fig. 8 Schematic diagram showing the metabolic heterogeneity and corresponding different characteristics of endometrial stromal cells and decidual cells.

with unique metabolic profiles presents notable technical challenges. This study reveals that decidual cell groups exhibit metabolic heterogeneity that varies with the degree of differentiation, and cells exhibiting high metabolism display enhanced cellular activity.

Decidual cells can be characterized by their enlarged round nuclei, increased number of nucleoli, dense-core secretory granules around the membrane boundary, accumulation of lipid droplets and glycogen in the cytoplasm, and an enlarged rough endoplasmic reticulum with the Golgi complex [13]. Hence, decidualization is an energy-intensive process that involves reprogramming of energy metabolism, including carbohydrate, lipid, and amino acid metabolism [12]. Here, we show significant changes in the metabolic profiles of stromal cells during the decidualization process. Glucose metabolism is activated, which aligns with previous studies [48, 49]. Additionally, amino acid-related metabolic pathways and sphingolipid metabolic pathways are significantly upregulated.

Furthermore, we illustrate that the presence of distinct decidual cells in the human endometrium, each displaying unique metabolic heterogeneity. Decidual cell clusters expressing high levels of decidual markers demonstrate increased sphingolipid metabolism activity. Uterine decidual cells with dysregulation in sphingolipid metabolism primarily die in early pregnancy, and abnormal sphingolipid metabolism leads to reduced proliferation of undifferentiated endometrial stromal cells [50]. Conversely, sub-clusters of decidual cells with lower decidual marker expression exhibit elevated amino acid metabolism pathway activity. Amino acid metabolism plays a central role in cellular metabolic homeostasis [51]. Previous data suggest that amino acids contribute significantly to conceptus growth and development through their effects on trophectoderm proliferation, differentiation, migration, and implantation [52]. Pregnant ewes and cyclic bovines exhibit significantly increased levels of free amino acids in uterine flushings compared to cyclic ewes and cyclic bovines [53, 54]. Downregulating genes involved in amino acid transport and metabolism impedes the progression of decidualization in both mouse and human endometrium [55, 56]. During early decidualization, active amino acid metabolism may contribute to stromal cells growth, nutrient accumulation, ultimately altering and maintaining their phenotype.

We implement the integration of decidual cells and trophoblast cells [57]. Our findings suggest that decidual cells with different metabolic features, engage in specific ligand-receptor interactions with distinct trophoblast sub-clusters. Notably, decidual cells with high metabolic activity exhibit heightened signal sending activity. We observe that NAMPT, the ligand of VISFATIN signaling pathway, is secreted by all decidual cell clusters and received by the iEVT and SCT. NAMPT exists in intracellular (iNAMPT) and extracellular forms (eNAMPT)

[58]. The extracellular form, eNAMPT, exerts neoplastic effects by acting as a pro-inflammatory cytokine, a proliferative and anti-apoptotic factor, as well as a promoter of angiogenesis, invasion, and metastasis [59]. Additionally, two decidual clusters secrete more ANGPTL signal which is received by the VCT-CCC, iEVT, and SCT cells. Notably, the expression levels of ANGPTL receptors along the pseudotime trajectory of trophoblasts exhibit an increase. ANGPTLs is a family of eight members (ANGPTL1 to ANGPTL8) [60]. Prior research suggests that ANGPTL1 negatively regulates angiogenesis, ANGPTL2 affects glucose metabolism, and ANGPTL4 impacts fat, lipid, or glucose metabolic homeostasis [61]. Our findings support the hypothesis that decidual cells likely play a role in regulating trophoblast invasion through the secretion of NAMPT, while decidual cells may influence the lipid and glucose metabolism of trophoblast cells through the secretion of ANGPTLs.

Based on scRNA-seq data, we conduct a prediction of cell-cell metabolite-sensor communications between decidual cells and trophoblast cells. Consistent with previous studies, our results demonstrate the presence of a substantial amount of 13-cis-retinoic acid in decidual cells [62, 63]. Notably, some decidual cells characterized by heightened sphingolipid metabolism activity and alanine, aspartate, and glutamate metabolism activity, secretes glutamine to the SCT and S1P to the VCT. Previous research has demonstrated that the sphingolipid metabolic pathway, particularly ceramides (Cer) and the enzymes involved in sphingosine and S1P production, are highly activated during early pregnancy in mice [15, 64]. Moreover, studies have shown that S1P enhances the invasion of immortalized human trophoblast cell lines through Hippo signal transduction [65]. The glutamine transporter SNAT5 is localized to the maternal-facing membrane of the SCT. Furthermore, glutamine can activate the mammalian target of rapamycin cell-signaling pathway, thereby enhancing protein synthesis and cellular proliferation in the placenta [66]. Overall, our results propose that decidual cells likely plays a role in providing nutrients to the SCT and regulating EVT invasion.

We observe distinct metabolic activities among subclusters of stromal cells and decidual cells, suggesting the presence of different metabolic subtypes within these populations. To further investigate this, we perform reclustering of stromal cells and decidual cells based on the expression profiles of metabolic genes. Remarkably, the clustering results obtained using metabolic genes are comparable to those obtained using highly variable genes. In a study by Bao et al., a unique subtype of decidual cells with high expression of genes involved in glycolysis was identified in decidua samples from both healthy donors and patients with recurrent miscarriage. This particular subtype was named glycolytic DSCs (glyDSCs), and it was predominantly found in patients with recurrent miscarriage [22]. Interestingly, we did not identify a similar group of decidual cells in our dataset, possibly indicating that glyDSCs are rare in the decidua of healthy individuals.

Finally, we observe that there are conserved changes in amino acid metabolism and sphingolipid metabolism in the uterus during the transition from cycling to pregnancy in placental mammals. Similar metabolic changes between the pregnant and non-pregnant uterus can be observed in mice, pigs, and cattle. Notably, uterine stromal cells in pigs and cattle do not undergo decidualization during pregnancy. Both humans and mice exhibit hemochorial placentation, characterized by direct contact between the maternal vascular space and fetal trophoblast cells [67]. Decidual cells can directly interact with trophoblast cells and regulate their activity. Cattle possess syndesmochorial placentation, where uterine luminal epithelial (LE) cells are maintained at the uterine-placental interface by being incorporated into trophoblast syncytial plaques. [68–70]. This type of placenta also allows trophoblast cells to contact endometrial stromal cells directly. In pigs, placentation is defined microscopically as epitheliochorial and macroscopically as diffuse, the uterine LE in pigs remains intact throughout pregnancy [69, 71]. Consequently, the endometrial stromal cells in pigs cannot directly interact with trophoblast cells. Instead, they may influence trophoblast cells by regulating the function of the epithelial cells. Genes associated with the alanine, aspartate, and glutamate metabolic pathway, glutathione metabolic pathway, and sphingolipid metabolism pathway are highly conserved in mammals. The similar endometrial metabolic changes observed before and after pregnancy in mammals with different types of placentas indicate the importance of these metabolic pathways in maintaining pregnancy. Further exploration is warranted to understand the divergence in roles and functions of these metabolic pathways across different mammals' endometrium during pregnancy, particularly in physiological stages such as maternal-fetal signaling, placental formation, and maintenance of endometrial function.

In summary, this study utilizes a combination of scRNA-seq and bulk RNA-seq data to elucidate the metabolic characteristics of endometrial stromal cells and decidual cells across distinct stages. Our findings reveal the presence of metabolic heterogeneity among subclusters of decidual cells and highlight that decidual cells with distinct metabolic features possess varying functions and engage in specific signaling with trophoblast cells. Future studies are required to elucidate the role of amino acid metabolism and sphingolipid metabolism in decidua development. By offering novel theoretical insights and avenues, this research lays the foundation

for further exploration into the distinctive attributes and roles of stromal cells and decidual cells, ultimately contributing to a better understanding of their significance in ensuring successful pregnancy.

Abbreviations

scRNA-seq	Single-cell RNA sequencing
cAMP	Cyclic adenosine monophosphate
GEO	Gene Expression Omnibus
DEGs	Differentially expressed genes
KEGG	Kyoto Encyclopedia of Genes and Genomes
GO	Gene Ontology
GSEA	Gene Set Enrichment Analysis
UMAP	Uniform Manifold Approximation and Projection
qRT-PCR	Real-time Quantitative polymerase chain reaction
TFs	Transcription factors
Endo	Endothelial cell
Epi	Endometrial epithelial cell
DS	Endometrial decidual stromal cell
Str	Endometrial stroma cell
Macro	Macrophage
NK	Nature killer cell
EVT	Extravillus trophoblast
N	Non-pregnancy
P	Pregnancy
iEVT	Invasive extravillous trophoblast cell
GC	Giant cells
VCT	Villous cytotrophoblast
VCT-CCC	Cytotrophoblast cell column VCT
SCT	Syncytiotrophoblast
OX	Oxidative phosphorylation
ML	Maximal likelihood
SH-aLRT	Shimodaira–Hasegawa-like approximate likelihood ratio test
MST	Minimum spanning tree
PAGA	Partition-based graph abstraction
MSigDB	Molecular Signatures Database
mIHC	Multiplex Immunohistochemistry
FFPE	Formalin fixation and paraffin embedding
AUC	Area under the curve

Supplementary Information

The online version contains supplementary material available at https://doi.org/10.1186/s12964-024-01763-y.

Supplementary Material 1

Acknowledgements
Our sincere thanks to Jie Zhang for support with multiplex immunohistochemical staining at Shandong university's Translational Medicine Core Facility of Advanced Medical Research Institute.

Author contributions
ZYJ, YW, and YZ performed the experiments and analyzed the data; YW and KS collected the human samples; ZYJ and JY designed experiments; KS and JY supervised the study; ZYJ and JY wrote the manuscript. The order of the co–first authors were assigned on the basis of their relative contributions to the study.

Funding
This work was supported by grants from the National Key Research and Development Program of China (2022YFC2702400), the National Natural Science Foundation of China (grant 32270906), the Natural Science Foundation of Shandong Province (grant 2022HWYQ-054), Taishan Scholars Program for Young Experts of Shandong Province (tsqn202103023).

Data availability
No datasets were generated or analysed during the current study.

Declarations

Ethical approval
Ethics approval for the collection and use of human endometrial samples was authorized by the Ethics Committee Review Board of Qilu Hospital, Shandong University (Permit No. KYLL-202203-011). All the recruited participants gave their written informed consent.

Consent for publication
Not applicable.

Competing interests
The authors declare no competing interests.

Received: 10 May 2024 / Accepted: 23 July 2024
Published online: 30 July 2024

References

1. Wang H, Dey SK. Roadmap to embryo implantation: clues from mouse models. Nat Rev Genet. 2006;7(3):185–99.
2. Cha J, Sun X, Dey SK. Mechanisms of implantation: strategies for successful pregnancy. Nat Med. 2012;18(12):1754–67.
3. Dey SK. How we are born. J Clin Invest. 2010;120(4):952–5.
4. Mori M, et al. The decidua—the maternal bed embracing the embryo—maintains the pregnancy. Semin Immunopathol. 2016;38(6):635–49.
5. Ochoa-Bernal MA, Fazleabas AT. Physiologic events of embryo implantation and decidualization in human and non-human Primates. Int J Mol Sci. 2020;21(6):1973.
6. Gellersen B, Brosens JJ. Cyclic decidualization of the Human Endometrium in Reproductive Health and failure. Endocr Rev. 2014;35(6):851–905.
7. Gellersen B, et al. Invasiveness of human endometrial stromal cells is promoted by decidualization and by trophoblast-derived signals. Hum Reprod (Oxford England). 2010;25(4):862–73.
8. Afshar Y, et al. Notch1 mediates uterine stromal differentiation and is critical for complete decidualization in the mouse. FASEB Journal: Official Publication Federation Am Soc Experimental Biology. 2012;26(1):282–94.
9. Pan-Castillo B, et al. Morphophysical dynamics of human endometrial cells during decidualization. Nanomed Nanotechnol Biol Med. 2018;14(7):2235–45.
10. Kelleher AM, et al. Uterine glands coordinate on-time embryo implantation and impact endometrial decidualization for pregnancy success. Nat Commun. 2018;9(1):2435.
11. Okada H, Tsuzuki T, Murata H. Decidualization of the human endometrium. Reproductive Med Biology. 2018;17(3):220–7.
12. Meng X, et al. Energy metabolism and maternal-fetal tolerance working in decidualization. Front Immunol. 2023;14:1203719.
13. Murata H, Tanaka S, Okada H. Regulators Hum Endometrial Stromal Cell Decidualization Biomolecules. 2022;12(9):1275.
14. Tsai J-H, et al. The fatty acid Beta-oxidation pathway is important for decidualization of endometrial stromal cells in both humans and mice. Biol Reprod. 2014;90(2):34.
15. Yang T, et al. Lipid metabolism and endometrial receptivity. Hum Reprod Update. 2022;28:858–89.
16. Mizugishi K, et al. Maternal disturbance in activated sphingolipid metabolism causes pregnancy loss in mice. J Clin Invest. 2007;117(10):2993–3006.
17. Lu L, et al. Expression and regulation of a Novel Decidual cells-derived estrogen target during decidualization. Int J Mol Sci. 2022;24(1):304.
18. Pique-Regi R, et al. A single-cell atlas of the myometrium in human parturition. JCI Insight. 2022;7(5):e153921.
19. Huang J, et al. Single-cell RNA sequencing reveals heterogeneity and differential expression of decidual tissues during the peripartum period. Cell Prolif. 2021;54:e12967.
20. Li S, et al. Metabolism drives macrophage heterogeneity in the tumor microenvironment. Cell Rep. 2022;39(1):110609.
21. Vento-Tormo R, et al. Single-cell reconstruction of the early maternal–fetal interface in humans. Nature. 2018;563(7731):347–53.
22. Bao S, et al. Single-cell profiling reveals mechanisms of uncontrolled inflammation and glycolysis in decidual stromal cell subtypes in recurrent miscarriage. Hum Reprod. 2023;38(1):57–74.
23. Stuart T, et al. Compr Integr Single-Cell Data Cell. 2019;177(7):1888–e190221.

24. Ritchie ME, et al. Limma powers differential expression analyses for RNA-sequencing and microarray studies. Nucleic Acids Res. 2015;43(7):e47.
25. Love MI, Huber W, Anders S. Moderated estimation of Fold change and dispersion for RNA-seq data with DESeq2. Genome Biol. 2014;15(12):550.
26. Qiu X, et al. Reversed graph embedding resolves complex single-cell trajectories. Nat Methods. 2017;14(10):979–82.
27. Wu T, et al. clusterProfiler 4.0: a universal enrichment tool for interpreting omics data. Innov. 2021;2(3):100141.
28. Browaeys R, Saelens W, Saeys Y. NicheNet: modeling intercellular communication by linking ligands to target genes. Nat Methods. 2020;17(2):159–62.
29. Wang Y et al. *iTALK: an R Package to Characterize and Illustrate Intercellular Communication* bioRxiv. 2019.
30. Jin S, et al. Inference and analysis of cell-cell communication using CellChat. Nat Commun. 2021;12(1):1088.
31. Rongbin Z et al. *MEBOCOST: Metabolic Cell-Cell Communication Modeling by Single Cell Transcriptome* bioRxiv. 2022.
32. Street K, et al. Slingshot: cell lineage and pseudotime inference for single-cell transcriptomics. BMC Genomics. 2018;19(1):477.
33. Wolf FA, Angerer P, Theis FJ. SCANPY: large-scale single-cell gene expression data analysis. Genome Biol. 2018;19(1):15.
34. Van De Sande B, et al. A scalable SCENIC workflow for single-cell gene regulatory network analysis. Nat Protoc. 2020;15(7):2247–76.
35. Shen W, et al. SeqKit: a cross-platform and Ultrafast Toolkit for FASTA/Q file manipulation. PLoS ONE. 2016;11(10):e0163962.
36. Katoh K. MAFFT: a novel method for rapid multiple sequence alignment based on fast Fourier transform. Nucleic Acids Res. 2002;30(14):3059–66.
37. Zhang D, et al. PhyloSuite: an integrated and scalable desktop platform for streamlined molecular sequence data management and evolutionary phylogenetics studies. Mol Ecol Resour. 2020;20(1):348–55.
38. Xu S, et al. Ggtree: a serialized data object for visualization of a phylogenetic tree and annotation data. iMeta. 2022;1(4):e56.
39. Letunic I, Bork P. Interactive tree of life (iTOL) v5: an online tool for phylogenetic tree display and annotation. Nucleic Acids Res. 2021;49(W1):W293–6.
40. Wang W, et al. Single-cell transcriptomic atlas of the human endometrium during the menstrual cycle. Nat Med. 2020;26(10):1644–53.
41. Korsunsky I, et al. Fast, sensitive and accurate integration of single-cell data with Harmony. Nat Methods. 2019;16(12):1289–96.
42. Zuo R-J, et al. Warburg-like Glycolysis and Lactate Shuttle in Mouse Decidua during early pregnancy. J Biol Chem. 2015;290(35):21280–91.
43. Samborski A, et al. Transcriptome changes in the Porcine Endometrium during the Preattachment Phase. Biol Reprod. 2013;89(6):134.
44. Zeng S, et al. Cell type-specific analysis of transcriptome changes in the porcine endometrium on Day 12 of pregnancy. BMC Genomics. 2018;19(1):459.
45. Samborski A, et al. Deep sequencing of the Porcine Endometrial Transcriptome on Day 14 of pregnancy. Biol Reprod. 2013;88(4):84.
46. Moreno-Moya JM, et al. Transcriptome of early embryonic invasion at implantation sites in a murine model. Reprod Fertility Dev. 2016;28(10):1487.
47. Walker CG, et al. Modulation of the maternal immune system by the pre-implantation embryo. BMC Genomics. 2010;11(1):474.
48. Frolova A, et al. Facilitative glucose transporter type 1 is differentially regulated by progesterone and Estrogen in murine and human endometrial stromal cells. Endocrinology. 2009;150(3):1512–20.
49. Huang J, et al. Protective role of GPR120 in the maintenance of pregnancy by promoting decidualization via regulation of glucose metabolism. EBioMedicine. 2019;39:540–51.
50. Ye Q, et al. Mechanisms of lipid metabolism in uterine receptivity and embryo development. Trends Endocrinol Metabolism. 2021;32(12):1015–30.
51. Porporato PE, et al. Metabolic changes associated with tumor metastasis, part 2: Mitochondria, lipid and amino acid metabolism. Cell Mol Life Sci. 2016;73(7):1349–63.
52. Li X, et al. Exposure to benzo[a]pyrene impairs decidualization and decidual angiogenesis in mice during early pregnancy. Environ Pollut. 2017;222:523–31.
53. Groebner AE, et al. Increase of essential amino acids in the bovine uterine lumen during preimplantation development. Reproduction. 2011;141(5):685–95.
54. Gao H, et al. Select nutrients in the Ovine Uterine Lumen. IV. Expression of neutral and acidic amino acid transporters in Ovine Uteri and Peri-implantation Conceptuses. Biol Reprod. 2009;80(6):1196–208.
55. Huang Z, et al. Cyclic adenosine monophosphate-induced argininosuccinate synthase 1 expression is essential during mouse decidualization. Mol Cell Endocrinol. 2014;388(1–2):20–31.
56. Wang X, et al. Positive regulation of decidualization by l-Type amino acid transporter 1 (lat1) in pregnant mice. Nutrients. 2016;8(11):704.
57. Arutyunyan A, et al. Spatial multiomics map of trophoblast development in early pregnancy. Nature. 2023;616(7955):143–51.
58. Navas LE, Carnero A. NAD + metabolism, stemness, the immune response, and cancer. Signal Transduct Target Therapy. 2021;6(1):2.
59. Dalamaga M, Christodoulatos GS, Mantzoros CS. The role of extracellular and intracellular nicotinamide phosphoribosyl-transferase in cancer: diagnostic and therapeutic perspectives and challenges. Metabolism. 2018;82:72–87.
60. Thorin E, et al. Angiopoietin-Like proteins: Cardiovascular Biology and Therapeutic Targeting for the Prevention of Cardiovascular diseases. Can J Cardiol. 2023;39:1736–56.
61. Oike Y, et al. Angiopoietin-like proteins: potential new targets for metabolic syndrome therapy. Trends Mol Med. 2005;11(10):473–9.
62. Berggren Söderlund M, Fex GA, Nilsson-Ehle P. Concentrations of retinoids in early pregnancy and in newborns and their mothers. Am J Clin Nutr. 2005;81(3):633–6.
63. Ozaki R, et al. Reprogramming of the retinoic acid pathway in decidualizing human endometrial stromal cells. PLoS ONE. 2017;12(3):e0173035.
64. Kaneko-Tarui T, et al. Maternal and embryonic control of uterine sphingolipid-metabolizing enzymes during murine embryo implantation. Biol Reprod. 2007;77(4):658–65.
65. Liao J, et al. Impaired sphingosine-1-Phosphate synthesis induces Preeclampsia by deactivating Trophoblastic YAP (Yes-Associated protein) through S1PR2 (sphingosine-1-Phosphate Receptor-2)-Induced actin polymerizations. Hypertension. 2022;79(2):399–412.
66. Wu G, et al. Impacts of amino acid nutrition on pregnancy outcome in pigs: mechanisms and implications for swine production. J Anim Sci. 2010;88(suppl13):E195–204.
67. Jiang X et al. A differentiation roadmap of murine placentation at single-cell resolution. Cell Discovery. 2023;9(1).
68. Peter AT. Bovine placenta: a review on morphology, components, and defects from terminology and clinical perspectives. Theriogenology. 2013;80(7):693–705.
69. Geisert RD and T.E, editor. Spencer. 2021, Cham, Switzerland: Springer.
70. Novosylna OVJSO, Structure, Functions. *Syncytia: Origin, Structure, and Functions* 2024.
71. Johnson GA, et al. Osteopontin expression in uterine stroma indicates a decidualization-like differentiation during ovine pregnancy. Biol Reprod. 2003;68(6):1951–8.

Publisher's Note